Received: 16 May 2023 | Revised: 4 November 2023 | Accepted: 2 December 2023

IET Radar, Sonar & Navigation

DOI: 10.1049/rsn2.12529

The Institution of Engineering and Technology WILEY

ORIGINAL RESEARCH

Multistatic radar distribution geometry effects on parameter estimation accuracy

D. Dhulashia | **M. A. Ritchie**

Department of Electronic and Electrical Engineering, UCL, London, UK

Correspondence

D. Dhulashia.
Email: dilan.dhulashia.15@ucl.ac.uk

Funding information

Thales Group; EPSRC, Grant/Award Number: EP/R513143/1

Abstract

An analysis of the parameter estimation uncertainty for the target location and velocity achievable using a single-transmitter-multiple-receiver multistatic radar system is presented. A framework for establishing measures of multistatic radar parameter uncertainties by expansion of the bistatic radar parameter uncertainty measures is presented for systems containing omnidirectionally radiating nodes. The methodology uses analytical methods based on the Cramér–Rao Lower Bounds applied to scenarios in a two-dimensional physical space with a single target exhibiting Doppler characteristics and a bistatic angle dependent radar cross-section. A set of geometric descriptors is proposed to characterise the system, and parameter uncertainty results are reported as a function of these descriptors. The results indicate that angular separation between the transmitter and the centre of the receiver distribution is of greater importance than the quantity of receivers within the system when low uncertainty estimation capabilities are desired, though a minimum of two receivers must be available. The proportion of receivers within the system which contributed information crucial to obtaining the minimum estimation uncertainty is reported for systems containing different quantities of receivers. It was observed that, as the total number of receivers available increased, the proportion of receivers required to achieve the minimal uncertainty level reduces significantly.

KEYWORDS

measurement uncertainty, multistatic radar, parameter estimation

1 | INTRODUCTION

Multistatic radar systems are a form of distributed radar sensing which utilise multiple monostatic or bistatic radar subsystems with a shared area of coverage. Such systems are comprised of multiple transmitter (Tx) and/or receiver (Rx) nodes. Beyond advantages including greater area coverage, low-probability of intercept, graceful degradation, and multiple perspective data collection, such systems also aim to achieve superior operational performance over conventional systems through the leverage of spatially distributed radar nodes capable of communication and data fusion [1]. While a full quantitative characterisation of multistatic radar performance is yet to be achieved, significant efforts have been made to show performance capabilities in the modalities of detection, parameter estimation, and tracking.

It is well understood that improvements in performance in many metrics may be obtained when data sharing across a distributed radar system is permitted. In Ref. [1], it was demonstrated how the location estimate accuracy for a target in the bistatic plane is improved though the use of a single-Tx-double-Rx multistatic system compared to a system using two radar stations with autonomous signal reception. The problem of quantitatively analysing a system's capability to accurately determine a parameter related to a target which has been detected is suited to being addressed by studying the variance of estimators for the parameter. Such a measure defines the amount of diversity which may be expected across a set of independent estimates for the parameter [2].

The Cramér–Rao Lower Bounds (CRLB) provide a minimum bound for the variance of an unbiased estimator for a

deterministic parameter. It has been shown how the CRLBs may be found with regards to the received radar data for a variety of parameters in Ref. [3]. The bistatic radar system topology is well established [4], and the parameter estimation problem in the context of bistatic radar parameters for Tx-Rx pairs within multistatic radar systems is addressed in Ref. [5]. The CRLB for the bistatic range and the velocity along the bistatic bisector were derived, and it was shown that geometry, waveform, and signal-to-noise ratio (SNR) are contributors to the quality of the parameter estimate. The optimal Tx-Rx pair for providing the lowest bistatic parameter uncertainty could then be selected from the nodes which make up the multistatic system.

In Ref. [6], the CRLB for the range, radial velocity, and direction of a point target is derived and considered for the case of the linearly frequency modulated (LFM) waveform. This work considered a monostatic radar architecture in a three-dimensional space using an active array capable of resolving directionality. The authors propose that a measure for the location uncertainty may be achieved by calculating the uncertainty volume which may be formed by the dimensions of the uncertainty in range and in angle. This is an example of the uncertainty in a higher dimension space being calculated through some combination of the uncertainties of parameters with lower dimensionality.

Work within existing literature has also looked to study the effects on best case parameter estimation as additional adversarial complexities become present in the scene [7]. Research of this kind highlights the difficulty in attempting to make a generalisable rule regarding the performance quality of a multistatic system for any parameter estimation problem; the particular geometry, environment, and characteristics will each have a significant impact on the performance and necessitate that analysis be carried out for a specific, well-defined scenario and system, or that a subset of the vast variable space be chosen to isolate the effects on the parameter estimation accuracy due to variations in only a few select variables.

Methods to determine optimal multistatic radar node geometries for parameter estimation accuracy of the position and velocity of a target in a two-dimensional space, based on the application of iterative optimisation algorithms, was demonstrated and verified in Ref. [8]. In this work, an approach was used to minimise the trace of the multiple parameter CRLB matrix, and Monte Carlo techniques were used to verify the proposed method. The application of the proposed method necessitates that Rx nodes be positioned based on prior knowledge about the performance of nodes which have already been placed. The practical implementation of such a method would therefore require control over the manoeuvrability of each Rx. The work specifically investigated a system consisting of a single Tx and four Rx nodes.

An analysis of some of the fundamental practical difficulties which arise when considering the data fusion and sharing required in multistatic systems is provided in Ref. [9]. The considerations which must be made depending on the cooperation level within the system are presented, along with a framework by which the CRLB on three geometric properties, namely the bistatic range, azimuth angle, and elevation angle, may be used to determine a volumetric uncertainty measure for the location parameter estimate of a target when the antennas in the radar system have a specific directionality. It is also reported that, in the case where antennas within the system are omnidirectional, the location estimate for a target must be fully determined using range information exclusively. Therefore, the location parameter estimate uncertainty is ultimately governed by the range parameter uncertainty from each constituent Tx-Rx pair contributing to a measurement. In such a case, the location parameter estimate has greater uncertainty compared to an equivalent scenario with directive antennas.

In Ref. [10], a signal model for the joint location and velocity estimation for a complex Gaussian extended target by a non-coherent multistatic radar was constructed and used to derive the CRLB for the parameter estimates. Theoretical and numerical results were presented assuming multiple Tx nodes capable of transmitting orthogonal waveforms, and it was reported that increasing the total number of nodes within the radar system (Tx and/or Rx) causes a reduction in the CRLB. Additionally, it was shown that the maximum likelihood (ML) estimate for both parameters of interest asymptotically converge to the true parameter value as the total number of nodes comprising the system increases.

Algorithms for the target localisation and velocity estimation for multistatic radar systems with differing architectures have been proposed in the existing literature, for example, [11], and the CRLB is derived to analytically show the efficiency of the estimator. An overview of the key general classifications for multistatic radar target localisation algorithms is mentioned in Ref. [12], and a joint method for target position and velocity estimation based on the principles is proposed and numerically assessed for scenarios containing a multiple-Tx-multiple-Rx system.

It has been proposed that typical and regular node distributions in multistatic radar systems may have worse performance for the objective of parameter estimation. Work in Ref. [13] employed a Pareto optimal layout for the radar nodes based on dynamic game theory. A volume calculated through the CRLB was used as a measure for the location parameter uncertainty in order to determine the performance of the proposed system layout, giving an example of a practical instance where a geometric space derived from the CRLB intervals has been used as a design analysis metric.

The concept of the swarm multistatic system architecture (single-Tx-many-Rx) was proposed in previous work; however, the parameter estimation problem was constrained to a consideration of only the bistatic parameters [14]. In this work, the Rx distribution within the physical containment space defined by the swarm geometry was random. The swarm performance at each instance was considered to be that of the best performing Rx (or some combination of several of the top performing Rxs), and the performance was then analysed over evolving scenarios.

This paper proposes a novel set of geometric parameters by which the distribution of a swarm multistatic radar system may be described at an abstracted level. Further, the work

extends the previous research in Ref. [14] by transitioning to concentrate on the equivalent joint-multi-perspective (or multistatic) parameters. A framework within which the multistatic parameter estimation capabilities of such a system may be analysed through the use of the bistatic parameter estimation capabilities of the constituent parts is described, and results demonstrating this usage are presented.

A full characterisation of the theoretical performance limitations of a multistatic system containing a single omnidirectional Tx and multiple omnidirectional Rx to carry out parameter estimation by leveraging preferable geometries has not yet been produced, particularly for systems with large node quantities where each Rx node is of relatively modest specification (i.e., a multistatic swarm system). The aim of this work is to present a methodology for quantifying the lower-bound uncertainty in target location and velocity estimates as established via the well-understood bistatic parameter uncertainties. Furthermore, the work seeks to understand and describe the relationship between the performance of parameter estimation and the topology of the multistatic swarm system and to determine a hierarchy of importance regarding the most critical topological components for an Rx swarm type architecture.

The rest of the paper is organised as follows: The theory regarding the relationship between bistatic and multistatic parameter estimates and the measures of parameter estimate uncertainty is given in Section 2. In Section 3, the methodology of the investigations carried out and the geometric parameters controlled are presented. The results from the simulations carried out are given in Section 4. Finally, Section 5 concludes the findings of the paper.

2 | THEORY

This work is interested in studying how the quality of estimates which can be obtained for two multistatic radar parameters, namely the target location and the target velocity, vary as a function of the topology of the radar system. These parameters are related to but fundamentally different from the bistatic parameters of bistatic range and component of target velocity in the direction of the bistatic bisector (bistatic velocity), both of which present their own estimate uncertainties. By considering the multistatic radar system as a collection of bistatic radar pairs with a common Tx and which are capable of sharing information between one another, it is possible to use the bistatic range and bistatic velocity estimation errors from several Tx-Rx pairs to form a measure for the estimate error for the location and velocity parameters. In this section, we present the theory explaining how this is possible.

Each Tx-Rx pair within the multistatic system gives both a bistatic range and a bistatic velocity estimation error. These errors are defined in the dimension along the bistatic bisector vector for each of the bistatic radar node pairs. It follows that, for a given point in space (at which a target is assumed to be positioned), several measures for the bistatic range or bistatic velocity estimate uncertainty would be available, each corresponding to a different bistatic pairs, and therefore, separated in angle from one another (i.e., along different directional vectors).

A measure for the accuracy of the estimates for the location of a target or a target's velocity can then be defined by the area of a region of uncertainty surrounding the parameter estimate in an appropriately representative vector space. The regions within the vector space whose area represents the estimate uncertainty are constructed by forming a perimeter using linear segments derived from the bistatic parameter estimation uncertainties. Therefore, in order to obtain the measure of accuracy for the location and velocity parameters, a quantitative measure for the bistatic parameter estimate uncertainty must first be expressed analytically, such that the measure quality from each bistatic pair within the multistatic radar system can sequentially be found, prior to constructing the region of uncertainty used to measure the estimation error of the multistatic parameters. A metric for the bistatic measure quality is chosen to be the CRLB which is computed from the likelihood function related to the two bistatic parameters being investigated.

The remainder of the theory section will begin by introducing the LFM waveform and finding the bistatic ambiguity function for it. Following this, the bistatic parameter CRLBs are presented, and an explanation to conceptually relate the joint-multi-perspective (multistatic) parameters to the bistatic parameters is given. Finally, an understanding of the geometric approach to finding the uncertainty for the multistatic parameters for both the target location and velocity, and for a single Rx system and for a multiple Rx system, is given.

2.1 | Linear frequency modulation (LFM) waveform

The LFM pulse is one of the most widely used waveforms and pulse compression techniques in radar. This signal is comprised of a uniform amplitude pulse which has been modulated linearly in frequency to achieve a wider bandwidth compared to an unmodulated frequency rectangular pulse. This enables finer range resolution to be achieved for an equivalent pulse length, thereby attaining improved range accuracy while maintaining pulse energy. A train of pulses may be formed by repeated transmission of the pulse. This enables the capacity to use Doppler processing through the determination of pulse-to-pulse phase variations. The complex envelope of a single LFM pulse is given by

$$s(t) = \frac{1}{\sqrt{T}} \mathrm{rect}\left(\frac{t}{T}\right) e^{j\pi \frac{f_B}{T} t^2}, \tag{1}$$

where T is the pulse length and f_B is the modulation bandwidth.

If the SNR of a received signal arising from the echoed reflection from a target is sufficiently high, the parameter estimation accuracy is primarily a function of the baseband signal waveform. In order to analyse the level of accuracy with which the parameters of interest may be measured using the

LFM waveform, the ambiguity function may be used [15]. The product of the ambiguity function with the SNR gives the log-likelihood function for the time-series given by the received signal samples. Here, a standardised definition of the ambiguity function is provided [16].

$$|\chi(\tau,\nu)|^2 = \left| \int_{-\infty}^{\infty} s(t)s^*(t+\tau)e^{j2\pi\nu t}dt \right|^2, \tag{2}$$

where τ and ν represent the time delay and Doppler frequency shift mismatch between the input signal to the matched filter and the nominal values used to characterise the design of the matched filter. Substitution of the waveform given by (1) into (2) gives the classical ambiguity function for a train of K identical pulses of the LFM waveform with a pulse repetition interval (PRI) of T_P, as [17].

$$|\chi(\tau,\nu)|^2 = \left| \left(1-\frac{|\tau|}{T}\right) \frac{\sin\left(\pi(\nu T - f_B\tau)\left(1-\frac{|\tau|}{T}\right)\right)}{\pi(\nu T - f_B\tau)\left(1-\frac{|\tau|}{T}\right)} \right.$$

$$\left. \cdot \frac{\sin(\pi\nu K T_P)}{K\sin(\pi\nu T_P)} \right|^2, \tag{3}$$

for $|\tau| \leq T$, or 0 outside this range.

2.2 | Bistatic radar parameter Cramér-Rao Lower Bounds

The quality of an estimator for a parameter may be quantified using the variance of the produced estimates. An estimator for a parameter which gives the minimal possible uncertainty is then the minimum variance estimator. The CRLB gives the theoretical best performance which may be achieved by a minimum variance unbiased estimator under idealised conditions. Therefore, finding the CRLB for a parameter will enable us to obtain a metric for the fundamental estimation accuracy of the parameter without regard for the practical details of the estimator used.

In this work, we use the uncertainty in the bistatic range and bistatic velocity estimation parameters of a target from multiple perspectives to obtain a measure for the uncertainty in the target location and velocity vector estimates. To this end, we must begin by finding the uncertainty in the bistatic parameters by finding expressions for the square root of the CRLB (RCRLB) for the bistatic range and bistatic velocity. These parameters may be understood by considering the general bistatic radar scenario as shown in Figure 1.

The bistatic radar scenario consists of a single Tx and single Rx node which are spatially separated by a baseline with distance, D_{Base}. Upon detection of a target, the bistatic radar system obtains an estimate for the bistatic range to the target, defined by the sum of the distances D_{Tx} and D_{Rx}. The velocity vector of the target is denoted $\vec{V}$, the bistatic bisector is

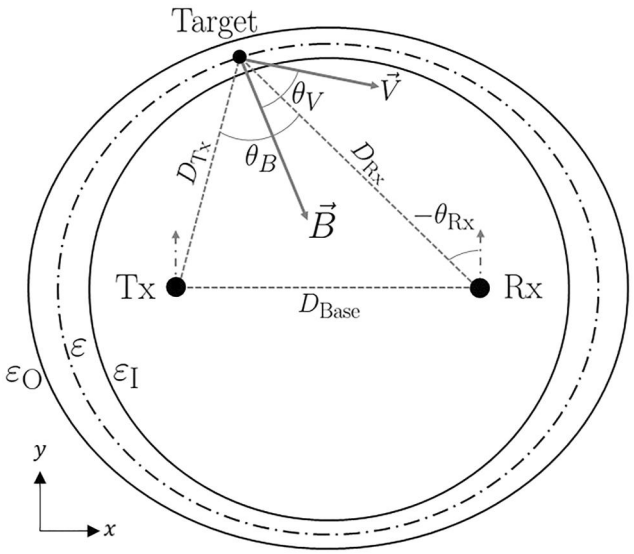

FIGURE 1 Bistatic radar geometry. Specific target is shown, along with bistatic iso-range ellipse corresponding to the target.

denoted $\vec{B}$, the bistatic angle is θ_B, the angle between the target velocity vector and the bistatic bisector is denoted θ_V, and the angle formed between the vector normal to the baseline with the line-of-sight (LOS) from the Rx to the target is denoted θ_{Rx}. No information regarding the direction to the target is known if the Tx and Rx are omnidirectional. Therefore, the estimate for the bistatic range only allows us to determine an iso-range ellipse focused on the Tx and Rx nodes, which, if there is no uncertainty in the bistatic range estimate, we say the target lies somewhere on (i.e., every point on the ellipse is a candidate for the true target location). The iso-range ellipse is shown by the scored line denoted ε in Figure 1. A specific target has also been illustrated in Figure 1 to exist at one particular candidate location without loss of generality.

When the uncertainty in the bistatic range to the target is considered, we must determine a confidence interval surrounding the estimate for the range within which we expect the true value for the bistatic range to exist. The size of this confidence interval (i.e., the difference between an upper and lower confidence value) is dependent on the geometry of the problem. Since each candidate location produces a different bistatic geometry, the size of the confidence interval surrounding the estimate for the bistatic range of a target is different for different candidate target positions. This is illustrated in Figure 1, where ellipses representing the points formed by the outer confidence boundary, ε_{O}, and the points formed by the inner confidence boundary, ε_{I}, are shown.

Quantitatively, the size of the confidence intervals may be given by the square root of the CRLB. The CRLB is given by elements within the inverse of the Fisher Information Matrix (FIM) which is calculated by taking the negative expectation of the partial derivative of the log-likelihood function with respect to the parameter vector, followed by the partial derivative with respect to the transpose of the parameter vector.

The likelihood function for both range and Doppler (or bistatic range and Doppler) parameter estimates for a received waveform is given by the product of the ambiguity function (or bistatic ambiguity function) with the SNR of the received signal. The ambiguity function considers, as variables, the mismatch between the known delay value (and Doppler value) associated with the matched filter design parameters and the unknown true value of the delay (and Doppler shift). This may be intuitively related to the likelihood function since a wider observed peak response in the ambiguity function leads to greater uncertainty regarding the precise delay or Doppler frequency value to which the peak relates [18].

We denote the CRLB for the bistatic range as ϱ^2 and for bistatic velocity as ϖ^2. These are then given explicitly by

$$\varrho^2, \varpi^2 = -2\mathrm{SNR}\left[\begin{array}{cc} \dfrac{\partial^2|\chi(\tau,\nu)|^2}{\partial\tau^2} & \dfrac{\partial^2|\chi(\tau,\nu)|^2}{\partial\tau\partial\nu} \\ \dfrac{\partial^2|\chi(\tau,\nu)|^2}{\partial\nu\partial\tau} & \dfrac{\partial^2|\chi(\tau,\nu)|^2}{\partial\nu^2} \end{array}\right]^{-1}_{[1,1],[2,2]} \tag{4}$$

The notation used here indicates that the computation of ϱ^2 and ϖ^2 utilise only the element of the inverse FIM at [1, 1] and [2, 2], respectively. It must be noted that each Tx-Rx pair in the system (i.e., each Rx) will have different CRLB values due to the differing SNR and geometry for each Rx. We therefore adopt the following notation such that the RCRLB for the bistatic range and bistatic velocity for the ith Rx, denoted Rx_i, are ϱ_i and ϖ_i, respectively, and that the numerical values for ϱ and ϖ may be found by numerical substitutions of the estimate for the delay and Doppler shift frequency.

As shown in Refs. [5, 19], the bistatic radar geometry may be accounted for by ensuring that the expressions for the delay and Doppler frequency shift are found in terms of the bistatic geometry characteristics. With reference to the general bistatic radar scenario in Figure 1, the delay and Doppler shift frequency are then given by

$$\tau = \frac{D_{\mathrm{Rx}} + D_{\mathrm{Tx}}}{c} = \frac{D_{\mathrm{Rx}} + \sqrt{D_{\mathrm{Rx}}^2 + D_{\mathrm{Base}}^2 + 2D_{\mathrm{Rx}}D_{\mathrm{Base}}\sin\theta_{Rx}}}{c}, \tag{5}$$

$$\nu = \frac{2f_c}{c}\left|\vec{V}\right|\cos\theta_V \sqrt{\frac{D_{\mathrm{Rx}} + D_{\mathrm{Base}}\sin\theta_{Rx}}{2\sqrt{D_{\mathrm{Rx}}^2 + D_{\mathrm{Base}}^2 + 2D_{\mathrm{Rx}}D_{\mathrm{Base}}\sin\theta_{Rx}}} + \frac{1}{2}}, \tag{6}$$

where f_c is the carrier frequency of the waveform, and c is the speed of light in a vacuum. These expressions enable us to find a form of the ambiguity function in Equation (2) which is written entirely in terms of the bistatic geometry parameters. A thorough treatment of this was given in Ref. [14]. It is then possible to compute (4) by taking the partial derivatives with respect to these variables, thus giving the bistatic parameter CRLBs.

If we consider an estimate for a target location given by $\vec{\psi}_{\mathrm{est}}$, we may also form an estimate for the bistatic bisector related to Rx_i which we denote $\vec{B}_i$. The location of the outer and inner confidence points for the target bistatic range as observed by Rx_i is then given, respectively, by

$$\vec{\alpha}_i', \vec{\alpha}_i = \vec{\psi}_{\mathrm{est}} \mp \frac{\varrho}{2}\vec{B}_i, \tag{7}$$

This confidence interval is a one-dimensional measure along the direction of the bistatic bisector. It provides no measure of the uncertainty of the target position in any other dimensions (i.e., no measure for cross-range uncertainty is given).

Similarly, if we consider an estimate for the target bistatic velocity to be given by $\vec{\gamma}_{\mathrm{est}}$ and use the estimate for the bistatic bisector obtained from the estimate for the target location, we may find the outer and inner confidence points for the target velocity are respectively given by

$$\vec{\beta}_i', \vec{\beta}_i = \vec{\gamma}_{\mathrm{est}} \pm \frac{\varpi}{2}\vec{B}_i, \tag{8}$$

These points exist in the velocity vector space but are also limited to the dimension given by the direction of the bistatic bisector. They therefore only provide information regarding the uncertainty in the estimate for the target velocity component in the direction of the bistatic bisector (i.e., the bistatic velocity) and do not give any information regarding the true direction or magnitude of the target velocity vector.

2.3 | Bistatic to multistatic parameters

In this paper, the bistatic parameter uncertainty metrics are used to establish a measure for the uncertainty of the analogous multistatic parameters. This can be considered more generally as the extension of the uncertainty of parameters which exist in a one-dimensional space, to the uncertainty of parameters existing in a two-dimensional space. The bistatic range to a target, measured from multiple spatially separated Rx nodes, can be used to obtain the location of the target relative to some common spatial frame (i.e., a common coordinate system). The bistatic range is a parameter within a single dimension. That is, it may only tell us the distance from the baseline centre at which the target lies; no information regarding the specific location may be obtained in the omnidirectional Tx and Rx case. On the other hand, the target location is a parameter within a two-dimensional space. It tells us both the distance and the direction in which the target is. The bistatic velocity of the target, measured from multiple spatially separated Rx nodes, may be used to determine the true target velocity vector relative to the common coordinate system. The bistatic velocity and the velocity vector are parameters in one and two dimensions, respectively.

In the following subsections, we describe the way in which the bistatic parameter uncertainty may be used to establish an

uncertainty in the equivalent multistatic parameters. For both the location and velocity parameters, this is split into two cases: the single-Tx-single-Rx case and the single-Tx-multiple-Rx (i.e., multistatic swarm) case. These must be treated separately since the underlying assumptions regarding the available prior information which may be useable in either case differ significantly. The assumptions regarding available measurement information in each case is described within the relevant subsections. In the following descriptions for the determination of the multistatic parameter uncertainty for a multi-Rx swarm, diagrams and reference are made to a specific case of two Rx nodes within the system without loss of generality.

2.4 | Location uncertainty

We begin the analysis of the location uncertainty by relating the bistatic range uncertainty to the location uncertainty. The bistatic range uncertainty must be analysed for a particular estimate of the target position (or equivalently, for a particular bistatic angle). Thus, the resulting measurement for the uncertainty gives a confidence interval along the direction of the bistatic bisector within which the target is expected to be situated, that is, the bistatic range uncertainty. However, this measure assumes that the bearing of the target is known with perfect precision. Therefore, the bistatic range uncertainty is equivalent to a measure of the location uncertainty if it is assumed that the target bearing is known perfectly.

2.4.1 | Single Rx

In the single Rx case, we may assume that an estimate for the target bistatic range is acquired; however, no information regarding the target bearing is available due to the omnidirectionality of the Tx and Rx antennas used. With this information, we may determine an iso-range bistatic ellipse corresponding to the estimate for the bistatic range, as shown in Figure 1. In the perfect instance (i.e., if there were no uncertainty in the measurement), the target would be assumed to lie at some point on this ellipse.

In order to analyse the location uncertainty, we may directly use the bistatic range uncertainty calculation methodology, noting that, this uncertainty measure is equivalent to a location uncertainty measurement if it is assumed that the target bearing is known perfectly. This may be done by sequentially assuming the target to be located at every possible position along the iso-range ellipse and analysing the bistatic range uncertainty for the given location.

Each assumed target position will give a bistatic range uncertainty measure. By summation of the bistatic range uncertainty measures for each position tested along the iso-range ellipse, we establish a measure for the total uncertainty in the target location. For a given selected target analysis position on the iso-range ellipse, we denote the point along the bistatic bisector which is at a distance half the RCRLB from the target estimate location such that it lies between the target and the baseline centre for the Tx-Rx pair, the inner coordinate. Similarly, we can denote an outer coordinate which is the point along the bistatic bisector a distance of half RCRLB from the target estimate position, but now such that it is on the opposite side of the target from the inner coordinate. Following Equations (7) and (8), the outer and inner coordinates for the Tx-Rx pair involving Rx_i for the bistatic range and bistatic velocity are denoted $\vec{\alpha}'_i$, $\vec{\alpha}_i$, $\vec{\beta}'_i$ and $\vec{\beta}_i$, respectively.

The set of the outer coordinates and the set of the inner coordinates will each form a closed boundary. The total target location uncertainty will then be the difference in the area contained by each of these boundaries, or equivalently, the area contained between these two boundaries.

A depiction of the region of uncertainty for the target location in the single Rx case, when the number of analysis points (i.e., possible target locations the bistatic range uncertainty is calculated for) tends to infinity is shown in Figure 2. The shaded area within the two boundaries depicts the uncertainty region.

2.4.2 | Multiple Rx swarm

In a two-dimensional space, it is possible to form an estimate for the target location if there exists more than one Rx in the system (i.e., we have a multistatic swarm). In the case of two Rxs, there will be two estimates for the target location given. For more than two Rxs, it is guaranteed that only one estimate for the target location will be generated.

A depiction for the two Rx cases is shown in Figure 3. This figure shows a general case where the target location has not been estimated. As such, there are two potential localities within which the target could exist, given by U_1 and U_2, and the dependency of the bistatic range uncertainty (i.e., the thickness of the elliptic bands) is non-constant. This results in the two uncertainty regions for the target location being lune-

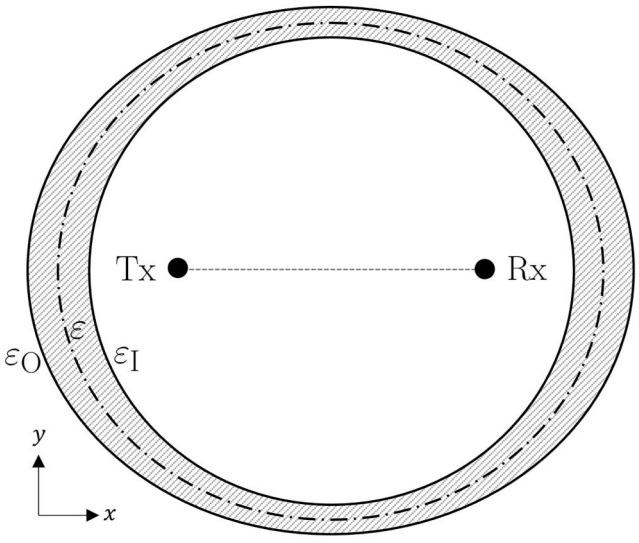

FIGURE 2 Target location uncertainty region for the single Rx case.

shaped. If an estimate for the target location is made and an estimate for the bistatic angle can be established, the bistatic range uncertainty can be treated as a constant (analysed only using the value of the bistatic angle estimate), and the lunes may be reduced to a parallelogram, as shown in Figure 4.

In the diagram shown in Figure 4 and in the subsequent analysis in this paper, we assume that, if multiple candidates for a target location estimate exist, a determination of which of the localities is correct is made such that only a single region needs to be analysed. For swarms consisting of more than two Rxs, only one target locality would be produced from the intersection of the iso-range ellipses, and determining a choice for $\vec{\psi}_{est}$ is trivial.

For each Tx-Rx pair in the swarm, we calculate the inner and outer coordinates along the corresponding bistatic bisector for the geometry formed by the pair with the estimated target location. Two perpendicular lines (referred to as uncertainty lines) may then be formed for each Tx-Rx pair in the system. These lines both have a direction which is normal to the bistatic bisector for the geometry formed by the Tx-Rx pair with the target estimate location. Depictions of this are shown in Figure 4, where the bistatic bisectors, inner and outer coordinates, and uncertainty lines for each Tx-Rx pair are shown. For Rx_i, the first uncertainty line, referred to as the outer uncertainty line and denoted L_i', passes through the outer coordinate for the Tx-Rx pair, $\vec{\alpha}_i'$, while the second uncertainty line, known as the inner uncertainty line and denoted by L_i, passes through the inner coordinate for the pair, $\vec{\alpha}_i$. Formally, the uncertainty lines are defined as follows:

$$\vec{L}_i', \vec{L}_i = \vec{\alpha}_i', \vec{\alpha}_i + t\vec{B}_{i\perp}, \tag{9}$$

where t is a variable to parameterise the line vectors, and $\vec{B}_{i\perp}$ is the directional unit vector perpendicular to the normalised bistatic bisector for Rx_i.

It is assumed that each Rx within the total set of all Rx in the system is uniquely located in space. Since the same Tx is used in all bistatic pairs, the uncertainty lines for a particular Rx will only be parallel to one another and will not be parallel to uncertainty lines from any other Rx. Therefore, each uncertainty line will intersect the two uncertainty lines resulting from every other Rx in the system. We denote the set of the coordinates of these intersection points $\check{C}$. The coordinate of the intersection between uncertainty lines $\vec{L}_i$ and $\vec{L}_j$ is represented by $\vec{C}_{L_i,L_j}$.

We may then use a subset of $\check{C}$, which we denote $\check{C}'$, in order to define a manifold in the vector space whose area represents the parameter uncertainty region. The manifold formed by connecting vertices contained in $\check{C}$ must be found such that no uncertainty lines exist within the area of the manifold. That is, only the coordinates from $\check{C}$ which result in the manifold of the smallest area which may be constructed through the use of segments from the different uncertainty lines are used and included in $\check{C}'$.

In the case of the two Rx swarms employed as the illustrative example system in this section, the locations of the four points which would be contained in $\check{C}$ are shown explicitly in the diagram in Figure 4 as follows: $\vec{C}_{L_1',L_2'}$, $\vec{C}_{L_2,L_1'}$, $\vec{C}_{L_1,L_2}$, and $\vec{C}_{L_2',L_1}$. In this instance, $\check{C}'$, which is used to define the minimal area manifold, is equivalent to $\check{C}$ (i.e., all four coordinates in $\check{C}$ contribute a vertex to the manifold).

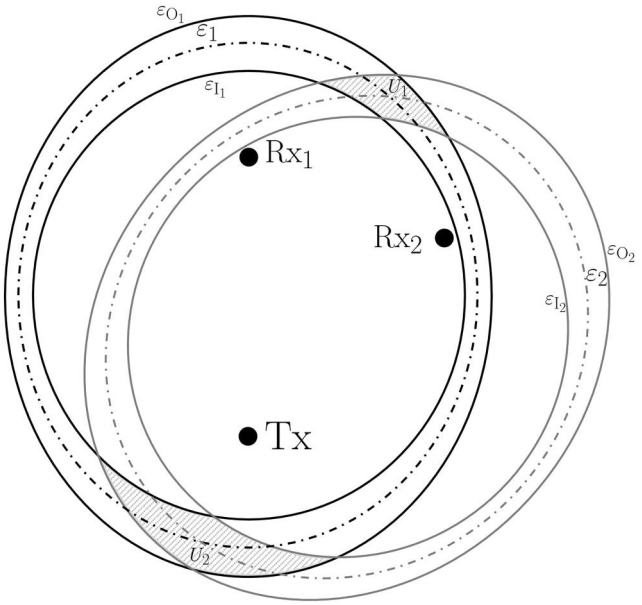

FIGURE 3 Target location uncertainty regions for multiple Rx swarms. Shown for two Rx swarms.

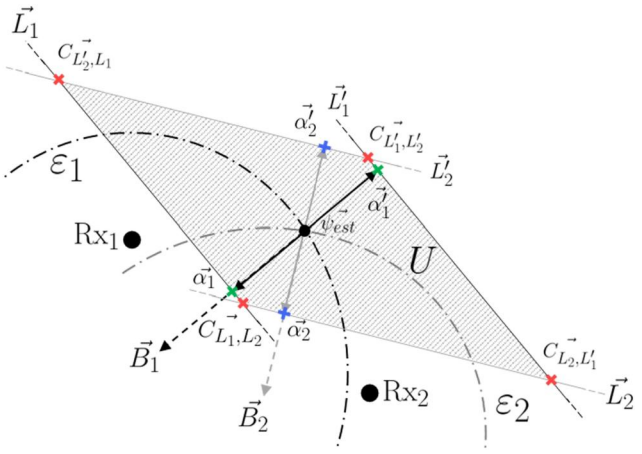

FIGURE 4 Analysis for determining the location uncertainty region for multiple Rx swarms. Shown for swarm with two Rxs.

2.5 | Velocity uncertainty

We begin the description of the technique for finding the velocity uncertainty by considering first the case with a single Rx system but assuming, unrealistically, an estimate for the location of the target exists. We then remove this assumption to give the general uncertainty for the single Rx system under realistic assumptions, before moving to the multi Rx case which builds on the techniques described in the single Rx case.

2.5.1 | Single Rx

It is assumed that, via the detection stage, an estimate for the radial speed (via Doppler frequency) is made at the Rx. If we assume that the target location is known, it follows that we know the bistatic bisector formed by the Tx-target-Rx geometry and therefore are able to determine the direction vector along which the radial speed component is directed, along with the polarity of the speed (i.e., towards or away from the Rx).

Using the known bistatic angle and geometry, we may determine the RCRLB on the bistatic velocity via (4). Furthermore, in an analogous fashion to the approach used for finding the location uncertainty area, we may use the estimate for the radial velocity along the bistatic bisector, denoted $\vec{V}_r$, to find the uncertainty interval for the true velocity value along the bistatic bisector direction. These values are represented by two coordinates in the velocity vector space and are found by (8), and as previously explained, are denoted by $\vec{\beta}'$ and $\vec{\beta}$ for the outer and inner bounds, respectively. This is shown in Figure 5.

Each point in the velocity vector space represents a particular target velocity vector. We must attempt to find the set of the velocity vectors which are viable candidates for the true velocity of the target. The span of this set then represents the uncertainty of the parameter estimate. Geometrically, this is equivalent to finding the area of the manifold in the vector space populated by the points representing the candidate velocity vectors.

Every point along the bistatic bisector between (and including) $\vec{\beta}'$ and $\vec{\beta}$ are viable candidates for the true target velocity vector. However, these candidate vectors only account for the uncertainty in the magnitude of the velocity and not the direction. The target velocity vector need not be in the direction of the bistatic bisector in order to produce a measured radial velocity component in this direction. The full set of the possible target velocity vectors which would result in an estimate for the radial velocity of the target along the bistatic bisector such that the observed magnitude lies between $\vec{\beta}'$ and $\vec{\beta}$ is then given by the points shown by the shaded region in Figure 5. This region is bounded in its extent in the direction of the bistatic bisector at the points of $\vec{\beta}'$ and $\vec{\beta}$, which is shown by the uncertainty lines given by $\vec{M}'$ and $\vec{M}$, given by

$$\vec{M}'_i, \vec{M}_i = \vec{\beta}'_i, \vec{\beta}_i + t\vec{B}_{i\perp}, \tag{10}$$

where t is again used to represent a variable to parameterise the line vectors. However, the uncertainty region extends infinitely in the direction normal to the bistatic bisector direction. It follows that the area of the uncertainty region (i.e., the shaded area representing the manifold) is then infinite.

We now reconsider the single Rx case with the removal of the assumption that the target location is known and instead assume that only an estimate for the bistatic range is available. We must then consider the methodology described thus far, but now for each candidate target location along the bistatic iso-range ellipse, in a similar fashion to that applied for the location uncertainty calculation for the single Rx case earlier in the section.

At each candidate target location, the uncertainty in the velocity parameter is infinite. It follows that the total uncertainty in any estimate for the velocity parameter must also be infinite, since it is comprised of the sum of infinite uncertainties obtained when each target location was considered separately and where these considerations are independent from one another.

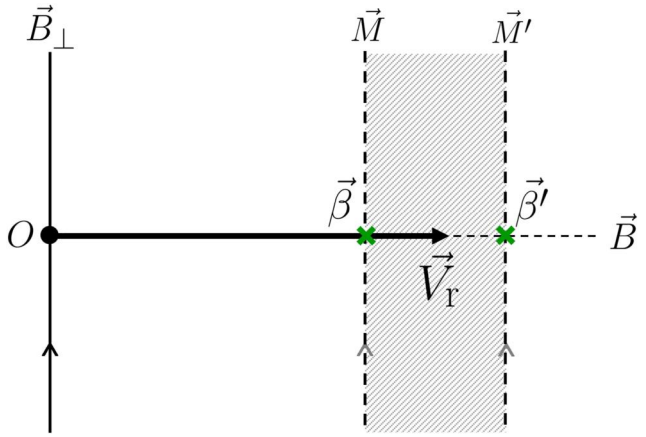

FIGURE 5 Possible velocity vectors which could cause an estimate for a particular radial velocity, given that the target position is known. Shown for positive radial velocity.

2.5.2 | Multiple Rx swarm

We now expand the theory outlined for the single Rx system to the case where multiple Rxs are present and illustrate this with the two Rx cases once again. It should be noted that, in the multiple Rx cases, as stated when considering the location uncertainty theory, it is assumed that an estimate for the target location can be and has been made.

Each Rx in multiple Rx systems acts as an independent single Rx system and will therefore produce a similar result as observed in the single Rx case. However, the bisector and perpendicular bisector will be oriented differently in the velocity vector space for each of the different Rx, as shown in Figure 6, since the geometry formed between the Tx, target, and each Rx will be unique. Therefore, the region of uncertainty in the velocity vector space (i.e., the shaded region containing all possible candidates for a target velocity vector) will be oriented differently for each Rx.

In this case, the uncertainty regions obtained from each Rx are not independent. The intersection area of the uncertainty regions from each Rx in the velocity vector space will then be the set of velocity vectors which could potentially correspond to the true target velocity vector when the observations from every Rx in the system is considered. A depiction of such an intersecting uncertainty region within the velocity vector space for a two Rx system is shown in Figure 6.

It is possible that, in a given scenario, some Rx within the swarm do not contribute additional useful information for the

formation of the parameter estimate (for either the location or the velocity parameter). This is said to occur if no portion of the perimeter which is found to bind the uncertainty region is shared with either of the outer or lower uncertainty lines produced by the Rx in question. An example depicting such a scenario is shown in Figure 7. This example is an expansion of the scenario depicted in Figure 4, such that a third Rx has now been included within the swarm. The vectors representing the bistatic bisector for each of the Rx are shown, along with the outer and inner uncertainty lines which run perpendicular to their associated bistatic bisector.

It can be seen in the example shown in Figure 7 that neither the outer nor inner uncertainty lines produced by the third Rx in the system (denoted $\vec{L}_3$ and $\vec{L}_3'$, respectively) have any contribution to the perimeter which bounds the minimal uncertainty region (i.e., adding a third Rx has not given any improvement in the parameter estimate accuracy compared to when two Rxs were using, as in Figure 4). In this instance, it may be concluded that, the total Rx in the swarm is three; however, only two of the Rx are contributing to finding the minimal parameter estimate uncertainty.

The probable causes for situations where particular Rx may not contribute to the parameter estimation improvement include the Rx being positioned such that the radiation scattering in the direction of the Rx is particularly unfavourable, such that a very low SNR is observed, or because the Rx is positioned such that the uncertainty lines it produces are highly similar to those already being formed by another Rx.

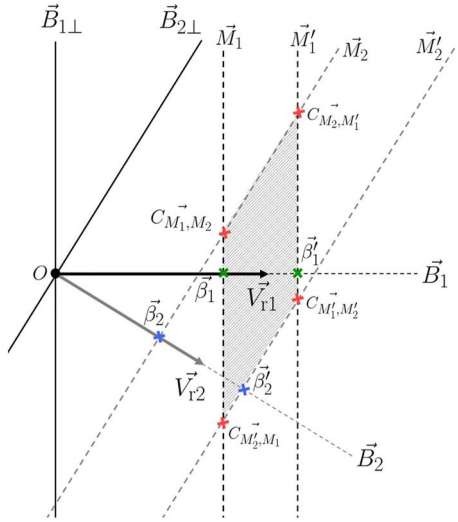

FIGURE 6 Translation of bistatic velocity component uncertainty to possible velocity vectors which could be responsible for the estimated bistatic velocity.

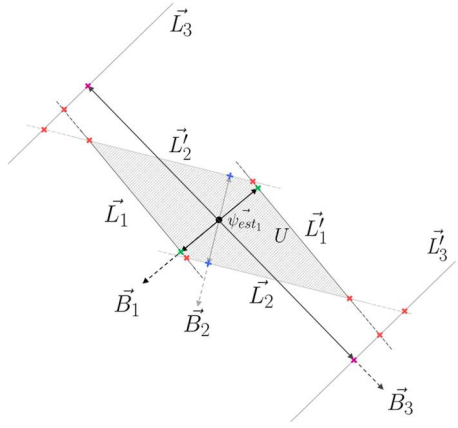

FIGURE 7 Example of target location estimation problem with a single-Tx-three-Rx system where one Rx is found to be non-contributing.

3 | METHODOLOGY

In this section, we present the general scenario setup which is used in order to perform the investigations. A description of the geometric characterisation of the swarm and the investigation variables is then provided before an outline of the steps involved in the investigation are given. Finally, descriptions of attributes used within the modelling are given, including the target radar cross-section (RCS) model, accounting for SNR variation across the different Rx in the swarm, and the specific waveform characteristics which were chosen.

3.1 | Multistatic radar architecture parameterisation

This research aims to investigate the effects of the characterisation of a multistatic swarm radar system on the uncertainty of the parameter estimates the system attains. To do this, we first must develop a set of characteristics which define the swarm such that we may vary these characteristics and determine the resulting effect which occurs on the parameter estimate uncertainty.

If we assume that a multistatic swarm radar system consists of a single Tx and multiple Rxs which are all located on the circumference of a semi-circular arc with equal angular separation between them, then an abstracted description of the swarm system may be given by the set of descriptors including the quantity of Rx within the swarm, the diameter of the semi-circular arc D_S, the distance of the centre of the swarm to the target D_{SC}, and the angle formed between the Tx, target, and the centre point of the swarm θ_{SC}. A depiction of the general investigation scenario layout is shown in Figure 8.

In general, a system of this nature would typically expect the distribution of its Rx nodes to be located in a stand-off type position from a target. It follows that the swarm diameter and distance of the centre of the swarm to the target may be combined into a ratio which we term the swarm centre to the target separation (SCTS) ratio. Explicitly, this is given as follows:

$$D_{SC} : D_S \tag{11}$$

It follows that, in general, we are only interested in cases where the ratio is > 1:1 (that is, the target may never lie within

the swarm, and the closest Rx to the target is always at least a distance of $\frac{D_{SC}}{2}$ from the target.

The individual Rx nodes within the swarm are defined to be located on the circumference of a semi-circular arc which is situated at a radius from the swarm centre (equal to half the swarm diameter). The arc is orientated such that the centre point of the arc is situated on the line formed between the centre point of the swarm and the target position.

In the case where the system contains only a single Rx, the Rx is positioned along the LOS from the swarm centre point to the target, at a distance equal to the swarm radius from the swarm centre. This is the closest point on the semi-circular arc (shown in Figure 8) to the target.

When the system contains n Rx, the position of Rx_i can be entirely described using an Rx positioning rule based upon the LOS from the swarm centre point to the target and the value of n. Since the range from the target to the swarm centre, D_{SC}, is fixed, and the swarm diameter, D_S, and the separation angle, θ_{SC}, are independent control variables which are selected, the position of the swarm centre, denoted P_{SC}, may be given by

$$P_{SC} = P_{\mathrm{Target}} + R_{(\theta_{SC})}\vec{P_{\mathrm{Target}}P_{\mathrm{Tx}}}, \tag{12}$$

where $R_{(\theta)}$ is the rotation matrix for an angle of θ, P_{Target} and P_{Tx} are the positions for the target and Tx, respectively, and $\vec{P_{\mathrm{Target}}P_{\mathrm{Tx}}}$ is the vector from the position of the target to the position of the Tx.

The position of Rx_i, denoted P_{Rx_i}, may then be described by

$$P_{\mathrm{Rx}_i} = P_{SC} + \frac{D_S}{2} R_{\left(\frac{\pi}{2} - \frac{\pi(i-1)}{n-1}\right)} \frac{\vec{P_{\mathrm{Target}}P_{\mathrm{Tx}}}}{\left|\vec{P_{\mathrm{Target}}P_{\mathrm{Tx}}}\right|}, \quad \text{where} \quad i \in [1, n]. \tag{13}$$

The ranges of values used for the independent variables in the investigation are listed in Table 1.

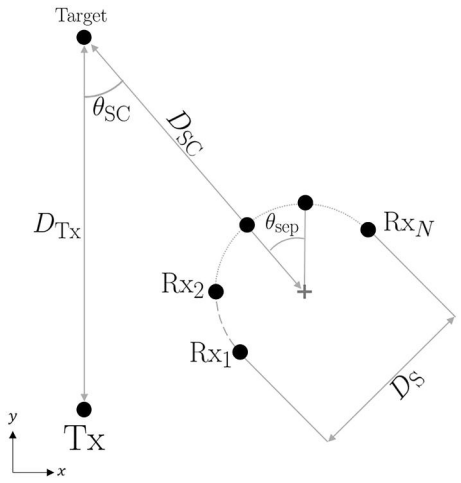

FIGURE 8 Depiction of an example of simulated scenario layout showing geometric controlled parameters for investigation.

The positions and dynamics of the Tx node and the target used were unchanged throughout the investigations. The Tx node was positioned at coordinate (0,0), meaning the distance D_{Tx} as shown in Figure 8 is fixed to 1 km. The target was positioned at coordinate (0,1000) and was assumed to have a velocity vector of (250,0). An assumption was made that, during the duration of the pulse train being used, the target position did not change significantly resulting in any effect imparted due to the target velocity being limited only to Doppler frequency shifts.

3.2 | Target RCS model

The SNR of a received radar signal has a dependency on the RCS of the target from which the signal is being reflected. The target RCS is determined by several factors, including target material, target shape, angle of incident radiation, and bistatic angle between target and radar nodes. In order to account for bistatic angle effects on target RCS while retaining generality regarding the target aspect angle, a model based on the bistatic RCS (BRCS) of a perfect electric conductor (PEC) sphere is employed in this work. For a given Tx-target-Rx geometry, the observed BRCS is assumed to be fixed. However, Rx which forms different bistatic geometries with the Tx and target will observe differing BRCS values. A plot of the BRCS relative to the monostatic RCS for the assumed target analysed using simulations with radiation of 1 GHz frequency is shown in Figure 9 and is used in the calculations of the SNR coefficient in the investigations within this work. The ratio of the sphere circumference to the wavelength is such that the target RCS can be considered to be within the optical region.

It should be noted that, in general, the RCS of a target is likely to vary greatly as a function of both the bistatic angle and

TABLE 1 Independent variable test values investigated.

Parameter	Test range	Step size
Target to swarm centre distance (D_{SC})[m]	500	-
Swarm rx quantity (n)[Nodes]	1–20	1
SCTS ratio	1,2,5,10:1	-
Angle to swarm centre (θ_{SC})[deg.]	0–180°	3°

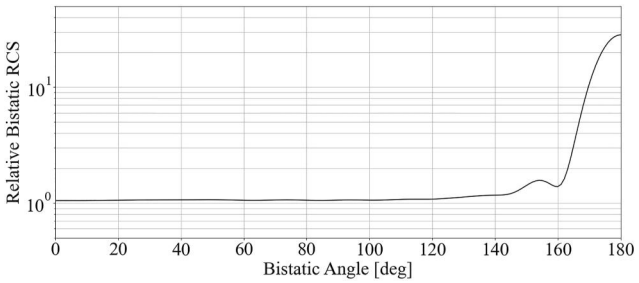

FIGURE 9 Bistatic Radar Cross-Section (BRCS) relative to monostatic Radar Cross-Section (RCS) of a perfect electric conductor (PEC) sphere of radius 1 m, analysed at frequency 1 GHz.

the aspect angle, and for particular targets, the BRCS can be significantly greater than the monostatic RCS [20]. Furthermore, even for simple targets such as that assumed in this work, the frequency of the radiation at which the RCS is analysed will have a significant impact on the observed values. Data for the BRCS of a PEC sphere is provided in Refs. [20, 21] and closely resembles the data which is used in the investigations carried out within this work.

3.3 | SNR at individual receivers

Since it is assumed that the parameter estimation problem necessitates that a detection of the target must have already been made, we may assume that an SNR of at least 10 dB (a fairly typical value at which detection may be considered possible for many radar systems) must be attained at each Rx within the system.

The precise SNR at each Rx in the swarm (i.e., the SNR at each Rx including the effects of signal power attenuation due to distance travelled, scattering due to observed BRCS, and Rx noise) is then found using the following approach. We begin by assuming an SNR level of 10 dB is achieved at the Rx furthest from the target when the target RCS and the Rx gain each take a value of unity, and the thermal noise level at all Rx is equal. It is then possible to determine the power which must be reflected from the target prior to accounting for actual observed BRCS in order to obtain the assumed SNR.

We may now remove the assumption of RCS equal to unity and instead determine the observed BRCS for the geometry formed with each individual Rx. The product of this BRCS value with the value obtained for the power reflected from a target prior to accounting for observed BRCS is then the representative of the true reflected power from the target in the direction of the Rx being considered. Finally, the specific distance between the target and the Rx under consideration may be used to reduce the reflected power by a factor proportional to the square of the distance. This results in the SNR at the Rx under consideration, having accounted for geometry, distance, and observed target BRCS. This procedure may be carried out for each Rx in the swarm to find the relative SNR at each for use in the computation of the CRLBs.

3.4 | Waveform characteristics

In this work, we are only interested in a single waveform type consisting of a train of LFM pulses. It is expected that the relationships which may be established between the geometric descriptors of the swarm and the parameter estimation capacity of the system should be independent of the specific waveform characteristics. As such, we chose a single set of waveform characteristics to use within the investigations carried out and note that, while modifying these parameters may improve or degrade the results from those reported here, the general relationships regarding the geometric parameters and the observed performance level should exhibit in a similar manner to that reported. The numerical values chosen for the waveform characteristics are listed in Table 2.

4 | RESULTS

This section is split into three parts. Firstly, we present the location parameter uncertainty region obtained in the single Rx case for each of the SCTS ratios and swarm angles tested. The second subsection presents the parameter uncertainty as a function of the geometric descriptors outlined in Section 3 for both the target location and velocity vector parameters. In the third subsection, the quantity of Rx within the swarms which were actually determined to contribute information used to determine the uncertainty region for each of the combinations of geometric descriptions is presented.

4.1 | Single Rx location uncertainty

As described in Section 2, the approach used to determine the parameter estimation uncertainty in the single Rx case necessitates that we assume no estimate for the parameter can initially be made. In the case of the location parameter uncertainty, we must therefore find the area of the region bounded between two closed boundaries as shown in Figure 2. We can intuitively expect that the order of magnitude of this area will be significantly greater than that of the uncertainty regions which will be calculated when the Rx quantity within the swarm is greater than one and the area of a manifold is being found. In the case of the velocity vector parameter estimation, it was established in Section 2 that the uncertainty will always be infinite if the Rx quantity is one. We therefore begin the results by presenting the parameter uncertainty region area obtained when a system containing a single Rx node is used for the range of SCTS ratios and swarm angles (equivalent to bistatic angle in the single Rx case). These results are shown in Figure 10. The results for the velocity uncertainty are not shown or discussed for the single Rx case due to their triviality.

From Figure 10, it may be observed that similar trends regarding the location uncertainty as a function of the swarm angle exist for each of the four SCTS ratios tested. In each case, the minimum uncertainty in the parameter estimate is observed when the swarm angle is close to zero degrees (i.e.,

TABLE 2 Values used for signal waveform characteristics.

Parameter	Value
Type	LFM
Bandwidth [MHz]	50
Pulse width [ms]	0.2
PRF [Hz]	1000
Carrier frequency [GHZ]	1
Train length [pulses]	64

pseudo-monostatic geometry), and generally increases with the angle at an accelerating rate. A local maxima is observed around 160° for each of the four SCTS ratios used, prior to the uncertainty eventually tending to infinity when the swarm angle approaches 180° (i.e., forward scatter in the case of the single Rx system).

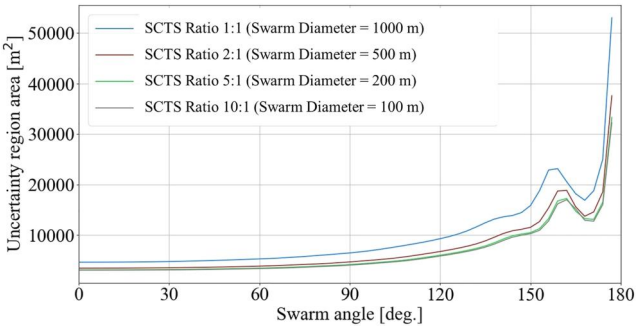

FIGURE 10 Location parameter uncertainty region area for the single Rx system.

4.2 | Multiple Rx parameter uncertainty

In this subsection, the results obtained for the measures of the uncertainty in the estimate for both of the parameters of interest for swarms containing more than one Rx are presented. These results are shown in the form of surfaces for each of the tested SCTS ratios. The surfaces have been grouped by the parameter such that those corresponding to the target location estimate uncertainty for each of the four SCTS ratios investigated are shown in Figure 11 and those corresponding to the target velocity estimate uncertainty is shown in Figure 12. In each surface plot, the control variables of the number of Rx in the swarm and the angle formed between the Tx, target, and swarm centre point are along the abscissa and the ordinate, respectively. The applicate then gives the uncertainty level for the parameter. The SCTS ratio values convert to real swarm

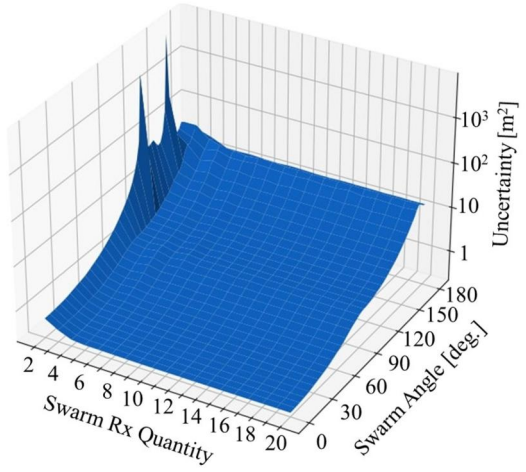

(a) SCTS ratio 1:1 (Swarm Diameter = 1000 m)

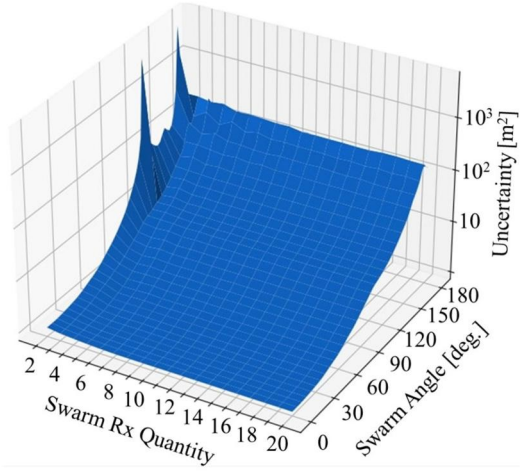

(b) SCTS ratio 2:1 (Swarm Diameter = 500 m)

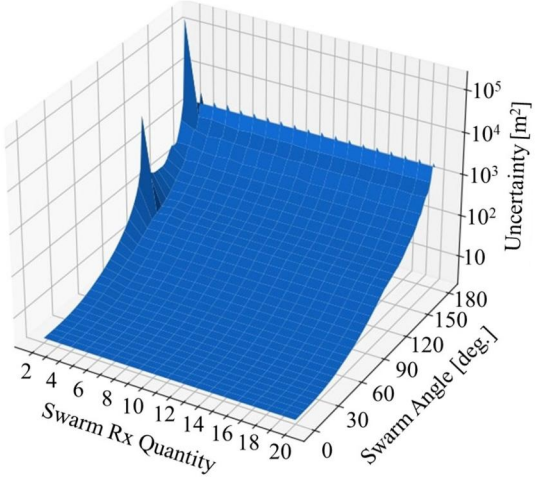

(c) SCTS ratio 5:1 (Swarm Diameter = 200 m)

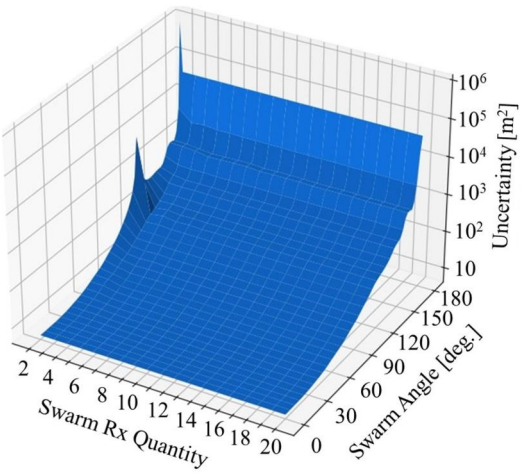

(d) SCTS ratio 10:1 (Swarm Diameter = 100 m)

FIGURE 11 Surfaces showing uncertainty for the target location estimate as the function of quantity of Rx in swarm and swarm centre LOS to the Tx LOS separation angle.

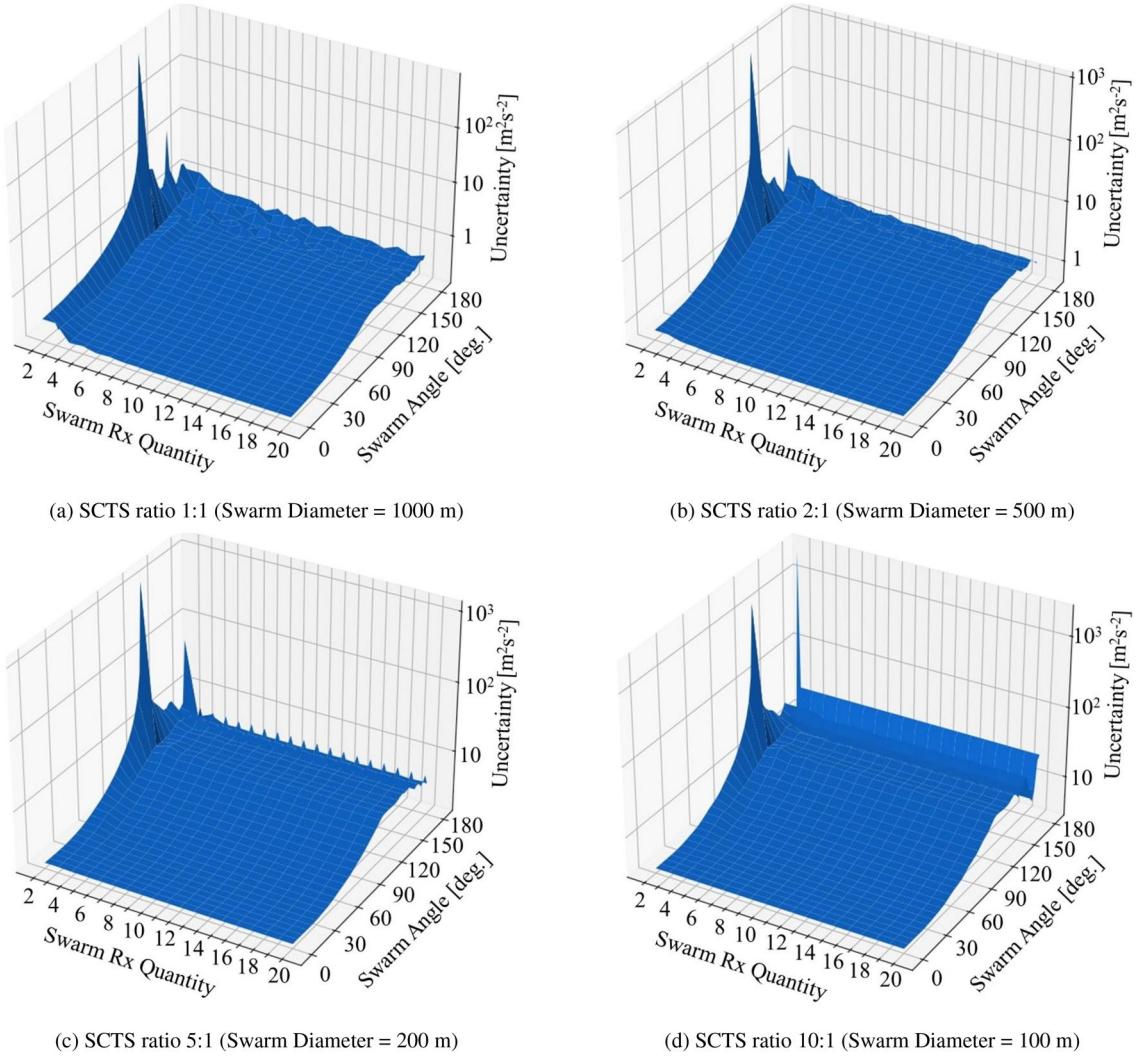

FIGURE 12 Surfaces showing uncertainty for target velocity estimate as function of quantity of Rx in swarm and swarm centre LOS to the Tx LOS separation angle.

diameters as follows: 1:1 = 1000 m, 2:1 = 500 m, 5:1 = 200 m, and 10:1 = 100 m.

We begin the discussion of the presented results by considering the target location estimate uncertainty surfaces, as shown in Figure 11. The general trends of the surfaces for each swarm diameter (SCTS ratio) appear to be similar, though, some differences can be observed. The improvements in the location parameter accuracy which are gained as the Rx quantity increases are of diminishing returns. That is, the location parameter accuracy is seen to improve with Rx quantity at a slower rate for greater swarm angles. Furthermore, for a given Rx quantity, the location parameter uncertainty increases as the swarm angle increases. The rate of this degradation with the swarm angle occurs at a slower rate for greater Rx quantities within the system.

The best performance is consistently achieved when a large Rx quantity is used and the swarm is positioned at a swarm angle close to zero degrees. Across all four of the surfaces related to the location parameter uncertainty, it can be observed that, for low Rx quantities, two pronounced peaks appear. The first of these peaks appears at a swarm angle of approximately 130° in all four surfaces, while the second peak appears to occur at approximately 165° in graph (a) of Figure 11 and continues to shift towards 180° for each subsequent surface (i.e., as SCTS ratio increases or swarm diameter decreases). This may be understood by considering that, as the swarm diameter decreases, the angular diversity between the different Rx within the system reduces. The system therefore behaves more similarly to a bistatic radar (i.e., a system with only one Rx) with a higher relative gain. In each of the four surfaces, a general trend showing a reduction in location uncertainty as the swarm angle increases, in particular for Rx quantities greater than four, can be clearly seen.

In each swarm diameter case, it can also be seen that the quantity of Rx in the swarm cannot counteract the negative impact of a poor swarm angle with regard to the location parameter estimation accuracy. That is, if a poor (wide) swarm angle geometry is used, increasing the Rx quantity will not

make up for the degradation in performance observed for the swarm diameter cases used. This is with the exception of the few angles at which the aforementioned local peaks occur. If these peaks are present when the Rx quantity is low, an additional Rx node may offer significant improvement in the parameter estimation accuracy. That said, a preferable geometry is typically seen to be more significant to achieving good location parameter estimation accuracy compared to the Rx quantity in the swarm.

By comparing the four surfaces relating to the location parameter estimation uncertainty, it can be deduced that, in general, as the swarm diameter decreases, the uncertainty in the location accuracy increases. Furthermore, this effect is more pronounced for wider swarm angles. Additionally, the reduction in location certainty as the swarm angle increases is much more significant for smaller swarm diameters (i.e., swarms where the Rx are more closely distributed).

We now discuss the results pertaining to the velocity parameter uncertainty, with reference to the surfaces in Figure 12. Similarly to the case of the location parameter, common trends may be observed across the four surfaces; however, the variation between the surfaces appears to be greater than that observed when comparing the corresponding four surfaces for the location parameter.

One significant difference when compared to the results surfaces for the location parameter uncertainty is that, while for small Rx quantities, a similar double peaked profile is exhibited across the swarm angle, it appears that the initial peak (occurring at a more acute swarm angle) reaches a greater uncertainty level than the second peak (occurring closer to the 180° swarm angle). An exception to this is seen in graph (b) of Figure 12, where the second peak, which occurs at a wider swarm angle, is the global peak.

Another key difference between the surfaces related to the location parameter uncertainty and those for the velocity vector parameter uncertainty is that, while the location parameter uncertainty surfaces are generally observed to continually increase at an accelerating rate as the swarm angle increases, the velocity vector uncertainty surfaces are observed to flatten at sufficiently wide swarm angles in all four of the graphs shown in Figure 12. For Rx quantities greater than two, it is only in surface (d) of Figure 12 that a significant rapid increase in velocity uncertainty is observed at swarm angles close to 180°.

Similarly to the location parameter uncertainty surfaces, a general trend is also observed in the surfaces for the velocity parameter uncertainty where, as the quantity of Rx in the swarm increases, the parameter uncertainty decreases, with diminishing returns for each additional Rx.

Furthermore, it is also observed in the case of the velocity parameter uncertainty that a preferable geometry (i.e., swarm angle) is always seen to be more significant to achieving good parameter estimation accuracy compared to the Rx quantity in the swarm. However, it is also seen that the relationship between uncertainty and swarm angle is more complicated for this parameter, particularly for swarm angles greater than 90°.

It should be noted that the relative differences observed between the location uncertainty levels compared to the velocity uncertainty levels for a given choice of geometric descriptor values are ultimately governed by the waveform characteristics. Different choices of waveform parameter values would lead to changes in the relative values observed between the two parameter uncertainties.

4.3 | Contributing receiver quantity

It is observed that the number of Rx which is actually contributing in the calculation of the uncertainty region area for either of the two parameters studied is not always equal to the total number of Rx within the swarm. That is, cases exist where it is found that no vertex within the minimum bounding polygon contains a contribution from the information from one or more of the Rx in the swarm. In such a case, we may say that there is some redundancy in the swarm—the same performance may be achieved if some of the Rx were completely removed.

In order to study this, the average number of contributing Rx nodes within the swarm versus the total number of Rx in the swarm has been shown in Figure 13. It should be noted that the Rx quantities used in this part of the investigation are such that $n \in \{1, 2, 3, \ldots, 20, 25, 30, \ldots, 100\}$.

For a given number of Rx in the swarm, the average number of contributing Rx is found by determining the number of Rx which is actually making a contribution to the uncertainty region area calculation for each particular swarm bistatic angle and SCTS ratio combination. These values are then averaged over all the independent variable combinations which were tested.

It can be seen from Figure 13 that, regardless of the total Rx quantity within the swarm, the average number of contributing Rx used to achieve the minimal location uncertainty is typically the same as the average number of contributing Rx used to achieve the minimal velocity vector uncertainty. Furthermore, it is seen that the number of Rx which is actually found to be contributing information used to find the minimal uncertainty region area begins to diverge further from the total quantity of Rx in the swarm as the Rx

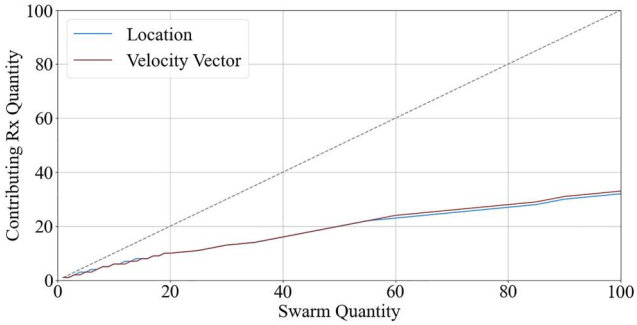

FIGURE 13 Average number of contributing Rx within the swarm versus the total number of Rx within the swarm.

quantity increases. In the case where 100 Rx were included in the swarm, only 32 and 33 Rx were found to contribute information used to construct the uncertainty region for the location and velocity vector parameter uncertainty, respectively.

While the reported findings suggest that the benefits which may be attained with respect to parameter estimation uncertainty by having additional Rx nodes within the swarm diminish as the quantity increases, it should be noted that this does not account for additional practicalities which may make higher quantities of Rx additionally beneficial. Examples of this include provision of greater area coverage, increased probability of obtaining multiple preferable perspectives to complex targets (e.g., extended targets consisting of multiple complex scatterers), increased probability of multiple Rxs with unobstructed LOS to the target in complex physical environments, and redundancy within the system which may offer graceful degradation in hostile environments.

5 | CONCLUSION

In this paper, a framework within which the bistatic radar parameter uncertainties for the bistatic range and bistatic velocity of a target may be used in a swarm multistatic radar system in order to analyse the uncertainties of the multistatic parameters of target location and velocity vector. The bistatic CRLBs are used as a basis for the analysis of the multistatic parameter estimation accuracy measures. The multistatic swarm radar architecture geometry is described in terms of the quantity of Rx, the swarm diameter, and the angle formed between the Tx, target, and Rx swarm centre, and results showing the parameter uncertainties as a function of these geometric descriptors are presented. The results showed that, given that the number of Rx in the swarm is greater than one, the angle formed between the Tx, target, and swarm centre point is of significantly greater influence on the parameter uncertainty for both target location and velocity vector than the Rx quantity in the swarm. Furthermore, the relationships between the rate of degradation in parameter uncertainty as a function of the swarm angle is greatly influenced by the swarm diameter; however, the general improvement and diminishing returns trend observed for the parameter uncertainty as a function of the Rx quantity holds in all cases are tested.

It was also observed that, regardless of the quantity of Rx within the swarm, the minimal parameter uncertainty could be achieved using a smaller proportion of the available Rx. From the results shown based on the range of Rx quantities used in the investigation, it is theorised that there could be a particular quantity of Rx above which no further improvement could be achieved (i.e., regardless of how many Rxs are included within the swarm, it could be found that only a specific sized subset of these provide useful information); however, it is expected that the particular Rx quantity above which no further accuracy improvement may be attained is likely to be highly scenario and context-dependent.

AUTHOR CONTRIBUTIONS

Dilan Dhulashia: Conceptualisation; Data curation; Formal analysis; Investigation; Methodology; Software; Validation; Visualisation; Writing – original draft; Writing – review & editing. **Matthew A. Ritchie**: Conceptualisation; Formal analysis; Funding acquisition; Methodology; Project administration; Supervision; Writing – review & editing.

ACKNOWLEDGEMENTS

This work was supported by Thales UK and the Engineering and Physical Sciences Research Council (EPSRC) under grant number: EP/R513143/1.

CONFLICT OF INTEREST STATEMENT

None.

DATA AVAILABILITY STATEMENT

Data is available on request from the authors.

ORCID

D. Dhulashia https://orcid.org/0000-0003-3401-9124
M. A. Ritchie https://orcid.org/0000-0001-8423-8064

REFERENCES

1. Chernyak, V.S.: Fundamentals of Multisite Radar Systems, 1st ed. Gordon and Breach Science Publishers (1998)
2. Kay, S.M.: Fundamentals of Statistical Signal Processing: Estimation Theory, 1st ed. Pearson Education (1993)
3. Van Trees, H.L.: Detection, Estimation and Modulation Theory, 1st ed. John Wiley & Sons, Inc. (1968)
4. Jackson, M.C.: The geometry of bistatic radar systems. IEE proceedings F (Communications, Radar and Signal Processing) 133(7), 604–612 (1986). IET Digital Library. https://doi.org/10.1049/ip-f-1.1986.0097
5. Greco, M.S., et al.: Cramér-Rao bounds and selection of bistatic channels for multistatic radar systems. IEEE Trans. Aero. Electron. Syst. 47(4), 2934–2948 (2011). https://doi.org/10.1109/taes.2011.6034675
6. Dogandzic, A., Nehorai, A.: Cramer-Rao bounds for estimating range, velocity, and direction with an active array. IEEE Trans. Signal Process. 49(6), 1122–1137 (2001). https://doi.org/10.1109/78.923295
7. Dhulashia, D., Temiz, M., Ritchie, M.A.: Jamming effects on hybrid multistatic radar network range and velocity estimation errors. IEEE Access 10, 27736–27749 (2022). https://doi.org/10.1109/access.2022.3157607
8. Griffin, B., et al.: Optimal receiver placement in staring cooperative radar networks for detection of drones. In: 2020 IEEE Radar Conference (Radar Conf 20), pp. 1–6 (2020)
9. Johnsen, T., Olsen, K.E.: Bi- and multistatic radar. In: Proc. Adv. Radar Signal Data Process, pp. 1–43 (2006). [Online]. https://www.sto.nato.int/publications/STO%20Educational%20Notes/RTO-EN-SET-086/EN-SET-086-04.pdf
10. He, Q., Blum, R.S., Haimovich, A.M.: Noncoherent MIMO radar for location and velocity estimation: more antennas means better performance. IEEE Trans. Signal Process. 58(7), 3661–3680 (2010). https://doi.org/10.1109/tsp.2010.2044613
11. Amiri, R., Behnia, F., Zamani, H.: Asymptotically efficient target localization from bistatic range measurements in distributed MIMO radars. IEEE Signal Process. Lett. 24(3), 299–303 (2017). https://doi.org/10.1109/lsp.2017.2660545
12. Yang, L., et al.: Joint position and velocity estimation of a moving target in multistatic radar by bistatic range, TDOA, and Doppler shifts. Int. J. Antenn. Propag. 2019, 1–7 (2019). Article ID 4943872, 7 pages. https://doi.org/10.1155/2019/4943872
13. Niu, C., Zhang, Y., Guo, J.: Pareto optimal layout of multistatic radar. Signal Process. 142, 152–156 (2018). https://doi.org/10.1016/j.sigpro.2017.07.017
14. Dhulashia, D., Temiz, M., Ritchie, M.A.: Performance of range and velocity estimation in a multistatic radar network with receiver swarms. In: Proc. IET Int. Radar Conf. 2022, pp. 447–452 (2022)
15. Woodward, P.M.: Probability and Information Theory with Applications to Radar. Artech House Publishers (1980)

16. Sinsky, A.I., Wang, P.C.P.: Error analysis of a quadrature coherent detector processor'. IEEE Trans. Aero. Electron. Syst. 10(6), 880–883 (1974). https://doi.org/10.1109/taes.1974.307900
17. Dash, D., Jayaraman, V.: Ambiguity function analysis for orthogonal-LFM waveform based multistatic radar. IEEE Sensors Letters 5(12), 1–4 (2021). https://doi.org/10.1109/lsens.2021.3129081
18. Levanon, N., Mozeson, E.: Radar Signals, 1st ed. John Wiley & Sons, Inc. (2004)
19. Tsao, T., et al.: Ambiguity function for a bistatic radar. IEEE Trans. Aero. Electron. Syst. 33(3), 1041–1051 (1997). https://doi.org/10.1109/7.599331
20. Cherniakov, M.: Bistatic Radar: Principles and Practice. John Wiley & Sons, Ltd. (2007)
21. Garcia, E., et al.: An efficient hybrid-scheme combining the characteristic basis function method and the multilevel fast multipole algorithm for solving bistatic RCS and radiation problems. Prog. Electromagn. Res. B 34, 327–343 (2011). https://doi.org/10.2528/pierb11062204

How to cite this article: Dhulashia, D., Ritchie, M.A.: Multistatic radar distribution geometry effects on parameter estimation accuracy. IET Radar Sonar Navig. 1–16 (2023). https://doi.org/10.1049/rsn2.12529